



**HAL**  
open science

# Quinoidal 2,2',6,6'-Tetraphenyl-Dipyranlydene as a Dopant-Free Hole-Transport Material for Stable and Cost-Effective Perovskite Solar Cells

Chao Shen, Marc Courté, Anurag Krishna, Shasha Tang, Denis Fichou

## ► To cite this version:

Chao Shen, Marc Courté, Anurag Krishna, Shasha Tang, Denis Fichou. Quinoidal 2,2',6,6'-Tetraphenyl-Dipyranlydene as a Dopant-Free Hole-Transport Material for Stable and Cost-Effective Perovskite Solar Cells. *Energy Technology*, 2017, *Perovskite Optoelectronics*, 5 (10), pp.1852-1858. 10.1002/ente.201700448 . hal-01629640

**HAL Id: hal-01629640**

**<https://hal.sorbonne-universite.fr/hal-01629640>**

Submitted on 6 Nov 2017

**HAL** is a multi-disciplinary open access archive for the deposit and dissemination of scientific research documents, whether they are published or not. The documents may come from teaching and research institutions in France or abroad, or from public or private research centers.

L'archive ouverte pluridisciplinaire **HAL**, est destinée au dépôt et à la diffusion de documents scientifiques de niveau recherche, publiés ou non, émanant des établissements d'enseignement et de recherche français ou étrangers, des laboratoires publics ou privés.



# Quinoidal 2,2',6,6'-Tetraphenyl-Dipyranylidene as a Dopant-Free Hole-Transport Material for Stable and Cost-Effective Perovskite Solar Cells

Chao Shen<sup>+</sup>,<sup>[a]</sup> Marc Courté<sup>+</sup>,<sup>[a]</sup> Anurag Krishna,<sup>[a]</sup> Shasha Tang,<sup>[a]</sup> and Denis Fichou<sup>\*</sup>,<sup>[a, b, c]</sup>

We report on the use of 2,2',6,6'-tetraphenyldipyranylidene (DIPO-Ph<sub>4</sub>), a large quinoidal planar  $\pi$ -conjugated heterocycle, as a simple, easy-to-synthesize, and efficient dopant-free hole-transport material in perovskite solar cells (PSCs). PSCs using pristine DIPO-Ph<sub>4</sub> show photon conversion efficiencies up to 10.1%, which is higher than a PSC utilizing dopant-free spiro-OMeTAD (5.1%). DIPO-Ph<sub>4</sub>-based PSCs exhibit a short-circuit current density of 19.52 mA cm<sup>-2</sup> and an open-

circuit voltage of 0.933 V, values that are superior to dopant-free spiro-OMeTAD and comparable to doped spiro-OMeTAD. These better performances find their origin in a higher HOMO level (-4.74 eV) and a much higher hole mobility ( $2 \times 10^{-2}$  cm<sup>2</sup> V<sup>-1</sup> s<sup>-1</sup>). Finally, PSCs based on DIPO-Ph<sub>4</sub> possess a superior stability compared to doped-spiro-OMeTAD-based devices when tested over 600 h.

## Introduction

Organic-inorganic halide perovskites, in particular methylammonium lead iodide (CH<sub>3</sub>NH<sub>3</sub>PbI<sub>3</sub>), recently emerged as highly efficient and low-cost materials for photovoltaic applications.<sup>[1-4]</sup> In the last few years the development of perovskite solar cells (PSCs) has been unprecedented, with power conversion efficiencies (PCEs) exceeding 20%.<sup>[5-8]</sup> In current PSC devices spiro-OMeTAD is the most commonly used hole-transport material (HTM).<sup>[9]</sup> However, its high cost due to a nontrivial synthesis combined with the need to mix it with various dopant materials is a major hindrance towards cost-effective PSCs. Therefore, it is mandatory to develop alternative HTMs with good transport properties that are easy to synthesize. A number of conjugated polymers, organic small molecules, and inorganic HTMs were reported.<sup>[10-12]</sup> Organic-small-molecule HTMs are preferred because they offer some unique advantages such as the possibility to tune their electronic properties by chemical design, few-steps, and low-cost synthetic pathways; solution processability; good stability; and its often environmental friendliness. Most of the reported HTMs are inferior to spiro-OMeTAD, but no HTM has yet clearly emerged in terms of cost, efficiency, and stability. Various classes of HTMs based on thiophene,<sup>[13]</sup> carbazole,<sup>[14]</sup> triazatruxene,<sup>[15]</sup> star-shaped molecules,<sup>[16]</sup> fluorinated indolo[3,2-b]indole,<sup>[17]</sup> or triptycene,<sup>[18]</sup> were recently investigated in PSCs. However, it appears that a number of these HTMs possess a non-planar molecular conformation that induces large intermolecular distances in the solid state; a typical example are HTMs based on triarylamine.<sup>[19-22]</sup> As a result, these HTMs suffer from a low hole mobility or conductivity in their pristine form that limits device performance.<sup>[23,24]</sup>

One promising strategy to improve charge transport is to use small  $\pi$ -planar conjugated molecules that assemble into

$\pi$  stacks in the solid state, giving rise to favorable intermolecular electronic coupling.<sup>[25]</sup> Only a few planar organic molecules were reported as dopant-free HTMs in PSCs, showing modest performances. For example, Kazim et al. reported on the use of pristine 6,13-bis(triisopropylsilylethynyl) pentacene (TIPS-pentacene) with a maximum efficiency of 11.51%.<sup>[26]</sup> Recently, Zou and co-workers reported the use of rubrene in a planar-inverted-configuration PSC device with a PCE as high as 15.83%.<sup>[27]</sup> In addition, two types of quinoi-

[a] Dr. C. Shen,<sup>+</sup> M. Courté,<sup>+</sup> Dr. A. Krishna, S. Tang, Prof. D. Fichou  
School of Physical and Mathematical Sciences  
Nanyang Technological University  
637371, Singapore (Singapore)  
E-mail: denisfichou@ntu.edu.sg

[b] Prof. D. Fichou  
Sorbonne Universités, UPMC  
Univ Paris 06, UMR 8232  
Institut Parisien de Chimie Moléculaire  
F-75005, Paris (France)

[c] Prof. D. Fichou  
CNRS, UMR 8232  
Institut Parisien de Chimie Moléculaire  
F-75005, Paris (France)

[\*] These authors contributed equally to this work.

Supporting Information for this article can be found under:  
<https://doi.org/10.1002/ente.201700448>.

© 2017 The Authors. Published by Wiley-VCH Verlag GmbH & Co. KGaA. This is an open access article under the terms of the Creative Commons Attribution Non-Commercial License, which permits use, distribution and reproduction in any medium, provided the original work is properly cited, and is not used for commercial purposes.

This publication is part of dual Special Issues on "Perovskite Optoelectronics", published in *Energy Technology* and *ChemSusChem*. Please visit the *Energy Technology* issue at <http://dx.doi.org/10.1002/ente.v5.10>, and the companion issue of *ChemSusChem* at <http://doi.org/10.1002/cssc.v10.19>.

dal small planar molecules were also reported as HTMs in PSCs, namely alkylated tetrathiafulvalene (TTF) derivatives (PCE = 11.03 %),<sup>[28]</sup> and 3,6-di(2*H*-imidazol-2-ylidene)cyclohexa-1,4-diene (PCE = 11.6 %).<sup>[29]</sup>

A widespread strategy to improve charge transport in HTMs consists of adding dopants of various types such as lithium bis(trifluoro-methanesulfonyl)imide (Li-TFSI), *tert*-butylpyridine (*t*-BP) and tris[2-(1*H*-pyrazol-1-yl)pyridine]cobalt(III) (FK 102).<sup>[30–32]</sup> However, these dopants are hydrophilic, which compromises solar cell stability, considering that the perovskite active layers are susceptible to moisture-induced degradation.<sup>[33]</sup> Finally, the use of dopants implies an additional step in the fabrication process and thus increases the final cost of the devices. To date, only a few dopant-free HTMs were reported, all of which are inferior to the ubiquitous spiro-OMeTAD in its doped form in terms of device performance and are often synthesized using complex and costly chemical procedures.<sup>[34–40]</sup> Hence, it is mandatory to design novel stable and dopant-free HTMs with appropriate properties.

2,2',6,6'-Tetraphenyldipyranilidene (DIPO-Ph<sub>4</sub>, Figure 1) is a simple small  $\pi$ -conjugated molecule consisting of two pyranilidene heterocycles interconnected through an exocyclic C=C double bond and bearing four peripheral phenyl groups on the 2,2',6,6' positions relative to the two O atoms.<sup>[41–43]</sup> Dipyranilidene derivatives are isoelectronic of tetrathiafulvalene and behave as strong  $\pi$  donors. In the solid state the large quinoidal planar  $\pi$ -conjugated structure of the molecule leads to a marked intermolecular face-to-face  $\pi$  stacking that is beneficial for charge transport. We recently reported on the hole mobility of DIPO-Ph<sub>4</sub> thin films as measured in field-effect transistors (FETs) that we recorded to be as high as  $\mu_{\text{h}} = 2 \times 10^{-2} \text{ cm}^2 \text{ V}^{-1} \text{ s}^{-1}$  with on/off ratio of the order of  $10^4$ .<sup>[44]</sup> Surprisingly, in this study we observed that the drain current/gate voltage ( $I_{\text{d}}/V_{\text{g}}$ ) transfer characteristics of these FETs present a clear hysteresis typical of a resistive memory effect. This memory effect was also observed when performing AFM at low voltages, and repeated write–read–erase–read cycles performed at low frequencies reveal a non-volatile memory effect in the form of high-resistance and low-resistance states.

We also recently demonstrated that DIPO-Ph<sub>4</sub> acts as an efficient hole-collecting interfacial layer in organic solar cells based on poly(3-hexylthiophene):phenyl-C<sub>61</sub>-butyric acid methylester (P3HT:PCBM).<sup>[45]</sup> Vacuum-deposited DIPO-Ph<sub>4</sub> thin films consist of densely packed and vertically aligned crystalline nanoneedles, a morphology that increases the con-

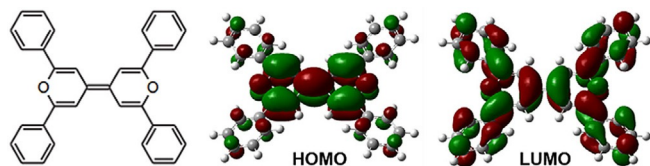


**Figure 1.** Left: chemical structure of DIPO-Ph<sub>4</sub>; middle and right: electronic density distribution of the HOMO and LUMO levels of DIPO-Ph<sub>4</sub> calculated by DFT using the B3LYP/631G method.

tact area with the adjacent active photovoltaic material and thus the rate of charge collection at this interface. Finally, note that in an earlier study we reported on the use of the sulfur analogue of DIPO-Ph<sub>4</sub>, namely 4,4'-bis(diphenyl-2,6-thiapyranilidene) (DIPS-Ph<sub>4</sub>), as a hole-collecting interlayer in organic solar cells.<sup>[46]</sup> and as a tunnel barrier in magnetic tunnel junctions.<sup>[47]</sup>

We report here on the use of DIPO-Ph<sub>4</sub> as a highly efficient and cost-effective HTM in PSCs. We show in particular that mesoscopic PSCs using DIPO-Ph<sub>4</sub> as the HTM possess a high short-circuit current  $J_{\text{SC}} = 19.52 \text{ mA cm}^{-2}$ , an open-circuit voltage  $V_{\text{OC}} = 0.933 \text{ V}$ , and a PCE as high as 10.1%. The simple chemical structure of DIPO-Ph<sub>4</sub> combined with a facile three-step synthesis (Scheme S1 in the Supporting Information) starting from inexpensive materials represent a major advantage with regard to large-scale device development.

## Results and Discussion

### Electronic properties of DIPO-Ph<sub>4</sub>

The experimental details of the synthesis of DIPO-Ph<sub>4</sub> were reported elsewhere and are briefly summarized in the Supporting Information (Scheme S1).<sup>[44]</sup> It consists of a straightforward three-step synthesis starting from inexpensive compounds. The UV/Vis absorption spectra of vacuum-deposited DIPO-Ph<sub>4</sub> thin films show an intense absorption in the visible region with an absorption edge around 640 nm corresponding to an optical band gap of 1.90 eV (Figure 2). In

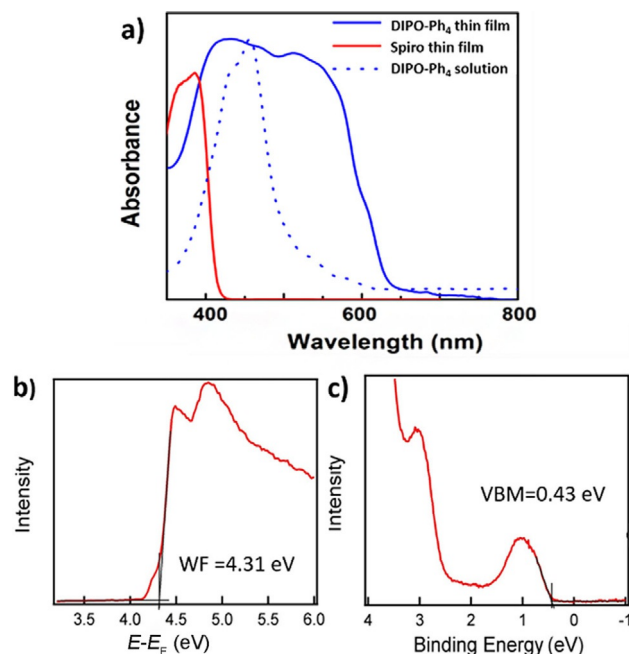


**Figure 2.** a) UV/Vis absorption spectra of DIPO-Ph<sub>4</sub> films (50 nm) and spiro-OMeTAD for comparison. b, c) UPS spectra of a 50 nm DIPO-Ph<sub>4</sub> thin film vacuum deposited on FTO. The onset of the curve is used to determine the Fermi level and the HOMO level of DIPO-Ph<sub>4</sub>.  $E_{\text{F}}$  = Energy of Fermi level, WF = work function, VBM = valence band maximum (spectrum (b) represents the photon energy minus the cut-off binding energy when the Fermi level is set to zero whereas spectrum (c) represents the binding energy).

comparison, spiro-OMeTAD only absorbs slightly in the visible range with an onset wavelength at 420 nm corresponding to an optical band gap of 2.98 eV. The HOMO level of DIPO-Ph<sub>4</sub> thin films is located at -4.74 eV as determined by ultraviolet photoelectron spectroscopy (UPS; Figure 2b and c) (HOMO = WF + VBM—the WF represents the working function and is directly related to the Fermi level of DIPO-Ph<sub>4</sub>, the VBM (valence band maximum) gives the value of the HOMO relative to the Fermi level; thus, the HOMO is obtained by the sum of VBM and WF). This HOMO is 0.37 eV higher than that of spiro-OMeTAD (-5.11 eV).<sup>[18]</sup> Furthermore, the HOMO energy level of CH<sub>3</sub>NH<sub>3</sub>PbI<sub>3</sub> is reported to be located at -5.44 eV, which is 0.7 eV lower than the HOMO of DIPO-Ph<sub>4</sub>. Clearly, DIPO-Ph<sub>4</sub> compares favorably with spiro-OMeTAD with a suitable energy level, for the use as an efficient HTM in PSCs (see the band diagram in Figure 3).<sup>[2]</sup> The electronic properties of DIPO-Ph<sub>4</sub>, together with those of spiro-OMeTAD for comparison, are summarized in Table 1. The electronic density distribution of frontier orbitals of DIPO-Ph<sub>4</sub> were calculated by density functional theory (DFT) using the B3LYP/631G method (Figure 1). The electron density in the LUMO wave function is delocalized over the whole molecular backbone, whereas the HOMO electron density is mainly localized on the dipyranylidene core. The HOMO level calculated by DFT of DIPO-Ph<sub>4</sub> (-4.03 eV) as well as spiro-OMeTAD (-4.48 eV)

(see Table 1) is slightly higher than the one obtained experimentally. The hole reorganization energy ( $\lambda_{\text{hole}}$ ) extracted from DFT calculations by withdrawing one electron from DIPO-Ph<sub>4</sub> is 0.285 eV, which is comparable to spiro-OMeTAD (0.16 eV), whereas the electron reorganization energy ( $\lambda_{\text{electron}}$ ) is 0.31 eV. Note that a small hole reorganization energy implies a fast transfer rate, which has consequences for the charge transport in the condensed phase.<sup>[48,49]</sup> In addition, vacuum-deposited DIPO-Ph<sub>4</sub> thin films are highly crystalline and possess a high hole mobility. FETs prepared in a bottom-gate/bottom-contact configuration show a typical p-type behavior with a hole mobility of  $\mu_{\text{H}} = 2 \times 10^{-2} \text{ cm}^2 \text{ V}^{-1} \text{ s}^{-1}$  and an on/off current ratio of  $6 \times 10^4$  (Figure S1). For comparison, the hole mobility of spiro-OMeTAD is reported to be in the range  $\mu_{\text{H}} = 10^{-4} - 10^{-5} \text{ cm}^2 \text{ V}^{-1} \text{ s}^{-1}$ ,<sup>[50]</sup> which is more than two orders of magnitude lower than that of DIPO-Ph<sub>4</sub>. Overall, the excellent electronic properties of the DIPO-Ph<sub>4</sub> thin films make it a potential candidate as an efficient HTM in perovskite-based solar cells.

#### PSCs using DIPO-Ph<sub>4</sub> as an HTM

Our PSC devices were fabricated in a typical configuration (FTO/TiO<sub>2</sub>/CH<sub>3</sub>NH<sub>3</sub>PbI<sub>3</sub>/HTM/Au) using mesoporous TiO<sub>2</sub> (mp-TiO<sub>2</sub>, Figure 4a). CH<sub>3</sub>NH<sub>3</sub>PbI<sub>3</sub> was prepared by performing a single-step method using a solvent treatment, forming shiny dark-brown films. DIPO-Ph<sub>4</sub> thin films were

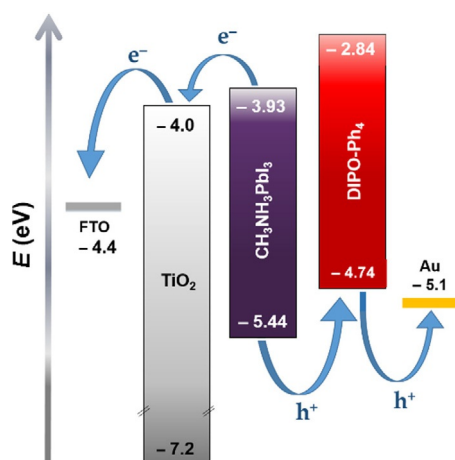


**Figure 3.** Band diagram of a perovskite solar cell using DIPO-Ph<sub>4</sub> as a dopant-free HTM.

HTM	$\lambda_{\text{onset}}$ [nm]	$E_{\text{g}}^{[a]}$ [eV]	$E_{\text{HOMO}}$ [eV]	$E_{\text{LUMO}}$ [eV]
			exp.	calc. <sup>[b]</sup>
DIPO-Ph <sub>4</sub>	637	1.90	-4.74	-4.03
spiro-OMeTAD <sup>[29]</sup>	416	2.98	-5.11	-4.48

[a] Optical band gap  $E_{\text{g}}$  obtained from the onset of absorption ( $\lambda_{\text{onset}}$ ). [b] HOMO calculated from DFT using the B3LYP/631G method. [c] LUMO calculated by  $E_{\text{LUMO}} = E_{\text{HOMO}} + E_{\text{g}}$ . [d] LUMO calculated from DFT using the B3LYP/631G method.

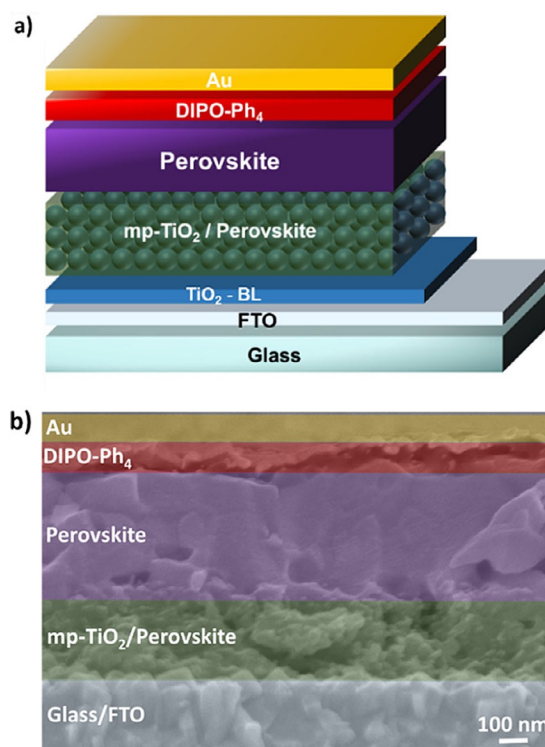


**Figure 4.** a) Device architecture of a mesoporous perovskite solar cell using DIPO-Ph<sub>4</sub> as the HTM. b) Cross-sectional SEM image of a typical device. The thicknesses of TiO<sub>2</sub> and perovskite are 250 and 400 nm, respectively.

deposited by thermal evaporation on top of the perovskite layer. Top-view SEM images reveal homogenous films (Figure S2). A chlorobenzene treatment allows the formation of large grains up to 500 nm in size. The X-ray diffraction pattern (Figure S3) reveals a polycrystalline structure with a strong orientation in the (110) plane. The UV/Vis spectrum shows a broad absorption on the visible range up to 800 nm, which is in good agreement with literature (Figure S4).<sup>[3]</sup> A cross-sectional SEM image of the device shows well-defined layers and clear interfaces (Figure 4b).

The  $J$ - $V$  characteristics of PSCs using either pristine DIPO-Ph<sub>4</sub> with various film thicknesses (30, 40, 50, 80 nm) or doped and undoped spiro-OMeTAD as HTMs were recorded under white-light illumination (AM 1.5G, 100 mW cm<sup>-2</sup>; Figure 5a). Performances of all devices are summarized in Table 2. PSCs without any HTM show poor characteristics with a PCE of only 4.5%. PSCs that integrate a dopant-free DIPO-Ph<sub>4</sub> thin film show higher performance.

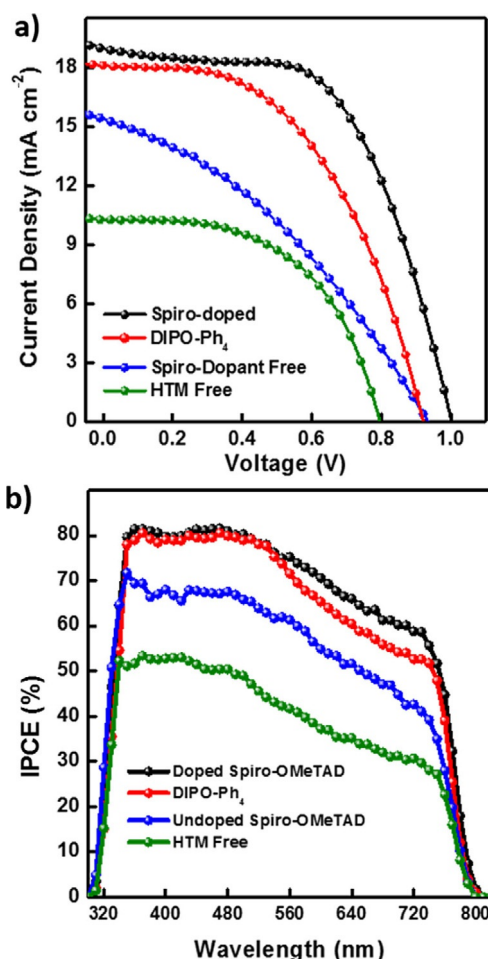


**Figure 5.** a)  $J$ - $V$  characteristics and b) IPCE spectra of perovskite solar cells fabricated using 40 nm-thick DIPO-Ph<sub>4</sub>, doped-spiro-OMeTAD, undoped-spiro-OMeTAD, and without HTM under illumination (AM 1.5G, 100 mW cm<sup>-2</sup>, active area = 0.2 cm<sup>2</sup>).

**Table 2.** Summary of device parameters  $V_{oc}$ ,  $J_{sc}$ , FF, and PCE of PSCs using either dopant-free DIPO-Ph<sub>4</sub>, doped spiro-OMeTAD, dopant-free spiro-OMeTAD, or without HTM.<sup>[a]</sup> For the sake of comparison, all reported values have been obtained in our laboratory.

HTM	Thickness [nm]	Area [mm <sup>2</sup> ]	$V_{oc}$ [V]	$J_{sc}$ [mA cm <sup>-2</sup> ]	FF [%]	PCE <sup>[b]</sup> [%]
no HTM	–	20	0.80	10.27	54.61	4.5 ± 0.5
dopant-free spiro-OMeTAD	100	20	0.94	15.38	35.58	5.1 ± 0.3
DIPO-Ph <sub>4</sub>	30	20	0.80	15.95	40.50	5.18 ± 0.4
	40	20	0.92	18.11	50.70	8.5 ± 0.3
	40	7	0.93	19.52	55.42	10.1 ± 0.4
	50	20	0.93	18.49	44.72	7.7 ± 0.9
	80	20	0.85	17.68	45.76	6.9 ± 0.6
doped spiro-OMeTAD	100	20	1.00	18.95	58.06	11.0 ± 0.8

[a] Measurements were performed under white-light illumination (AM 1.5G, 100 mW cm<sup>-2</sup>). [b] The standard deviation of PCEs is based on experimental results obtained for six devices of each PSC type.

The optimized thickness of DIPO-Ph<sub>4</sub> film is 40 nm (Figure 6). For this configuration, the highest PCEs are as high as 10.1% with a short-circuit current density  $J_{sc}$  = 19.52 mA cm<sup>-2</sup>, an open-circuit voltage  $V_{oc}$  = 0.93 V, and a fill factor FF = 55.4%. For thinner DIPO-Ph<sub>4</sub> films (30 nm), the  $J_{sc}$ ,  $V_{oc}$  and FF values are slightly reduced to 15.95 mA cm<sup>-2</sup>,

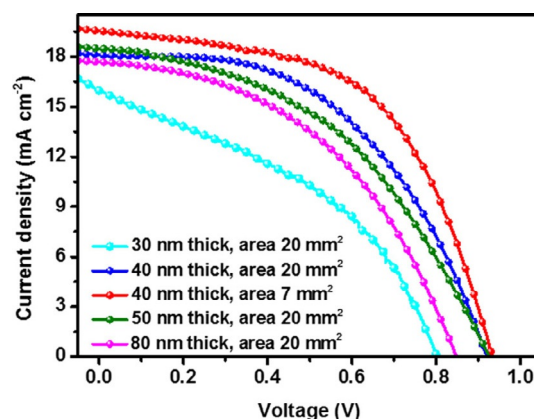


**Figure 6.**  $J$ - $V$  characteristics of PSCs using different DIPO-Ph<sub>4</sub> thicknesses from 30 to 80 nm. The active areas of the PSCs are either 20 or 7 mm<sup>2</sup>. The  $J$ - $V$  curves are recorded under white-light illumination (AM 1.5G, 100 mW cm<sup>-2</sup>).

0.80 V, and 40.5%, respectively. This suggests that for low DIPO-Ph<sub>4</sub> thicknesses, that is, below 30 nm, the films are inhomogeneous and the interface with the perovskite layer is of lower quality. For DIPO-Ph<sub>4</sub> films thicker than 40 nm (i.e., 80 nm), we also observe a lower  $V_{oc}$  (0.85 V) due to a higher recombination rate in DIPO-Ph<sub>4</sub>. In comparison, devices using dopant-free and doped spiro-OMeTAD as the HTM show a PCE of 5.1% and 11.0%, with a  $J_{sc}$  of 15.38 and 18.95 mA cm<sup>-2</sup>, respectively. Thus, PSCs using DIPO-Ph<sub>4</sub> present  $J_{sc}$  values that are higher than those with dopant-free spiro-OMeTAD.

The origin of the improved  $J_{sc}$  of DIPO-Ph<sub>4</sub>-based PSCs lies in its higher HOMO level (−4.74 eV) compared to that

of spiro-OMeTAD ( $-5.44$  eV) in combination with a hole mobility that is higher by two to three orders of magnitude. The higher HOMO level allows a stronger driving force for charge transfer from the perovskite to the HTM. However, PSCs using DIPO-Ph<sub>4</sub> show a slightly lower  $V_{oc}=0.93$  V than those with doped spiro-OMeTAD ( $V_{oc}=1.00$  V). As  $V_{oc}$  depends on multiple factors such as the splitting of the Fermi levels for photogenerated charges, the recombination rate, and the energetics of the device,<sup>[18]</sup> the slightly lower  $V_{oc}$  might be due to the higher HOMO level. The lower FF compared to doped spiro-OMeTAD can be attributed to the high series resistance of the DIPO-Ph<sub>4</sub> films.

Incident photon-to-electron conversion efficiency (IPCE) spectra (Figure 5b) are in agreement with the  $J-V$  curves, revealing similar trends. The integrated  $J_{sc}$  well match with  $J_{sc}$  measured under white-light illumination and fits entirely the absorption spectra of the perovskite. The similar shapes of the IPCEs for all samples suggest that light absorption by the HTM has a negligible effect on the performance. Howev-

er, as DIPO-Ph<sub>4</sub> thin films strongly absorb over most of the visible range up to approximately 650 nm, the contribution of DIPO-Ph<sub>4</sub> in the overall photocurrent needs to be considered. Therefore, we fabricated TiO<sub>2</sub>/DIPO-Ph<sub>4</sub> bulk heterojunctions (i.e., free of perovskite), in which the DIPO-Ph<sub>4</sub> thin film is expected to function both as the light-harvesting material and the HTM. The recorded photocurrent is as low as  $J_{sc}=0.09$  mA cm<sup>-2</sup>, showing that only UV light contributes to  $J_{sc}$  (Figure S5), which excludes any contribution from DIPO-Ph<sub>4</sub> light absorption in the  $J_{sc}$  of PSCs.

Stability is crucial for the development of PSCs, moisture being one of the major causes for their degradation. Spiro-OMeTAD needs to be doped with materials that are hygroscopic and therefore induce device degradation. We now demonstrate that the use of a dopant-free small molecule HTMs leads to more stable PSC devices.

As shown in Figure 7, the devices fabricated using DIPO-Ph<sub>4</sub> exhibit a much slower degradation compared to spiro-OMeTAD-based devices. The devices were kept at a relative

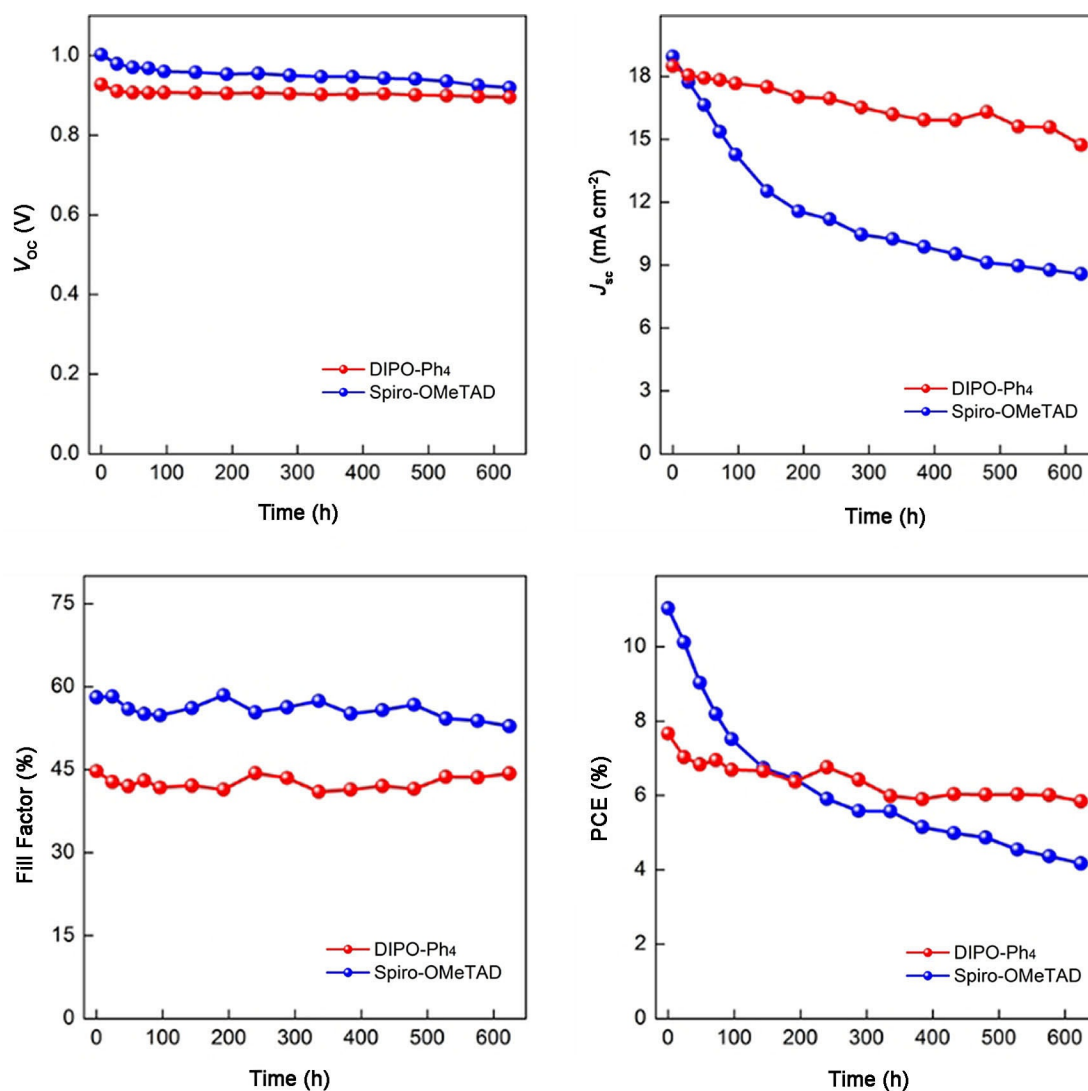


**Figure 7.** Stability of PSC parameters using doped spiro-OMeTAD and DIPO-Ph<sub>4</sub> as HTM. Cells are stored in a dry box at room temperature with a relative humidity of roughly 30%. Measurements were performed under white-light illumination (AM 1.5G, 100 mWcm<sup>-2</sup>).

humidity of roughly 30% and were tested for 600 h. The DIPO-Ph<sub>4</sub>-based PSCs show only an approximately 20% decrease in PCE compared to an approximately 60% degradation with spiro-OMeTAD. This enhanced stability in DIPO-Ph<sub>4</sub> devices can unambiguously be attributed to the absence of deliquescent additives or dopants. These encouraging results suggest that dipyranylidene can be used as a core for dopant-free HTMs for stable PSCs.

## Conclusions

The quinoidal dipyranylidene DIPO-Ph<sub>4</sub> (2,2',6,6'-tetraphenylidipyranylidene) has been inserted as a dopant-free hole-transport material (HTM) in perovskite solar cells (PSCs). DIPO-Ph<sub>4</sub>-based PSCs show power conversion efficiencies (PCEs) of up to 10.1%, which is two times higher than those obtained with undoped spiro-OMeTAD (5.1%), still retaining short-circuit current densities and open-circuit voltages comparable to those of doped spiro-OMeTAD-based devices. Moreover, DIPO-Ph<sub>4</sub>-based devices showed better stability compared to spiro-OMeTAD devices at a relative humidity of 30%. We are confident that with further optimization of device parameters and by understanding the interfacial characteristics, there can be further significant improvement in the device performance. The straightforward chemical synthesis and the high charge carrier mobility make DIPO-Ph<sub>4</sub> a potential candidate to substitute the more expensive spiro-OMeTAD in PSCs. This work also lays the ground for a strategy to design and develop new dipyranylidene-based HTMs for stable and cost-effective organic solar cells.

## Experimental Section

### Fabrication of the DIPO-Ph<sub>4</sub>/perovskite solar cells

Fluorine-doped tin oxide (FTO, < 14 Ω/□, 3 mm thick) substrates were etched to form the desired pattern, which were subsequently cleaned by sonication in 2% Hellmanex aqueous solution, deionized water, and ethanol, respectively. A thin compact layer of TiO<sub>2</sub> as a blocking layer between FTO and perovskite was deposited by atomic layer deposition. The mesoporous-TiO<sub>2</sub> layer composed of 30-nm-sized particles was deposited by spin coating at 6000 rpm for 30 s using a commercial TiO<sub>2</sub> paste (Dyesol DSL 30 NRD) diluted in ethanol (2:7, weight ratio). After drying at 70 °C, the TiO<sub>2</sub> films were gradually heated to 500 °C, baked at this temperature for 30 min, and then cooled to room temperature. An organic-inorganic perovskite CH<sub>3</sub>NH<sub>3</sub>PbI<sub>3</sub> was deposited by performing a single step method using a solvent treatment.<sup>[3]</sup> Following the spin-coating step, the samples were annealed at 100 °C for 30 min. Spiro-OMeTAD was dissolved in chlorobenzene (100 mg mL<sup>-1</sup>) and spin-coated on top of the perovskite layer. Additives such as Li-TFSI, *t*-BP, and FK 102 were added to the above solution according to a protocol described previously.<sup>[7]</sup> DIPO-Ph<sub>4</sub> was deposited on the perovskite by evaporation under high vacuum ( $P=10^{-4}$  Pa) at a slow rate of 0.2 Å s<sup>-1</sup> as monitored by a quartz microbalance (Inficon, X TM/2). The substrates were placed in a thermal evaporator for Au deposition using shadow masking. The thickness of the Au electrode was about 100 nm, and an active area of 0.2 cm<sup>2</sup> was defined by the overlap of TiO<sub>2</sub> and Au.

## Characterization

The TiO<sub>2</sub> thickness was determined by using an Alpha-Step IQ surface profiler (KLA-Tencor). The morphology was characterized with a field-emission scanning electron microscopy (FESEM, FEI SIRION). Absorbance spectra were measured by using a UV/Vis spectrophotometer (Shimadzu, UV-2501PC). Cyclic voltammetry measurements were performed using an electrochemical station (model CHI760d) with a three-electrode cell composed of glassy carbon as working electrode and Pt electrode as auxiliary electrode. An Ag/AgCl (sat. KCl) electrode was used as a reference electrode. The electrolyte consisted of 0.5 mM of the organic HTM and 0.1 M Bu<sub>4</sub>NClO<sub>4</sub> in DMF. The scan rate was 200 mV s<sup>-1</sup>. The photocurrent-voltage characteristics of the solar cells were measured by means of an electrochemical workstation (Zennium, Zahner, Germany) under AM 1.5G solar simulator (100 mW cm<sup>-2</sup>, Newport, calibrated with a silicon reference cell). The IPCE spectra were measured using a 300 W xenon lamp and a monochromator controlled by TracQ Basic software (QEPVSI-b Measurement System, Newport). All DFT calculations were performed using Gaussian 09 software. The geometry of the DIPO-Ph<sub>4</sub> was optimized before calculating the HOMO and LUMO levels, as well as the electronic density distribution energies using the basis sets B3LYP/631G.

## Acknowledgements

This research is supported by the Academic Research Fund (AcRF) Tier 2 (MOE2014-T2-1-132) issued by the Ministry of Education, Singapore.

**Keywords:** cost-effective • dopant-free • hole transport • perovskite solar cells • stability

- [1] M. M. Lee, J. Teuscher, T. Miyasaka, T. N. Murakami, H. J. Snaith, *Science* **2012**, *338*, 643–647.
- [2] H. S. Kim, C. R. Lee, J. H. Im, K. B. Lee, T. Moehl, A. Marchioro, S. J. Moon, R. Humphry-Baker, J. H. Yum, J. E. Moser, M. Grätzel, N. G. Park, *Sci. Rep.* **2012**, *2*, 591.
- [3] J. Burschka, N. Pellet, S.-J. Moon, R. Humphry-Baker, P. Gao, M. K. Nazeeruddin, M. Grätzel, *Nature* **2013**, *499*, 316–319.
- [4] G. Xing, N. Mathews, S. Sun, S. S. Lim, Y. M. Lam, M. Grätzel, S. G. Mhaisalkar, T. C. Sum, *Science* **2013**, *342*, 344–347.
- [5] A. Kojima, K. Teshima, Y. Shirai, T. Miyasaka, *J. Am. Chem. Soc.* **2009**, *131*, 6050–6051.
- [6] M. Liu, M. B. Johnston, H. J. Snaith, *Nature* **2013**, *501*, 395–398.
- [7] H. Zhou, Q. Chen, G. Li, S. Luo, T. B. Song, H.-S. Duan, Z. Hong, J. You, Y. Liu, Y. Yang, *Science* **2014**, *345*, 542–546.
- [8] N. J. Jeon, J. H. Noh, Y. C. Kim, W. S. Yang, S. Ryu, S. I. Seok, *Nat. Mater.* **2014**, *13*, 897–903.
- [9] A. Gheno, S. Védraïne, B. Ratier, J. Bouclé, *Metals* **2016**, *6*, 21.
- [10] N. J. Jeon, H. G. Lee, Y. C. Kim, J. Seo, J. H. Noh, J. Lee, S. I. Seok, *J. Am. Chem. Soc.* **2014**, *136*, 7837–7840.
- [11] A. Krishna, A. C. Grimdale, *J. Mater. Chem. A* **2017**, <https://doi.org/10.1039/C7TA01258F>.
- [12] L. Calió, S. Kazim, M. Grätzel, S. Ahmad, *Angew. Chem. Int. Ed.* **2016**, *55*, 14522–14545; *Angew. Chem.* **2016**, *128*, 14740–14764.
- [13] T. Krishnamoorthy, F. Kunwu, P. P. Boix, H. Li, T. M. Koh, W. L. Leong, S. Powar, A. C. Grimdale, M. Grätzel, N. Mathews, S. G. Mhaisalkar, *J. Mater. Chem. A* **2014**, *2*, 6305–6309.
- [14] K. Lim, M.-S. Kang, Y. Myung, J.-H. Seo, P. Banerjee, T. J. Marks, J. Ko, *J. Mater. Chem. A* **2016**, *4*, 1186–1190.

- [15] K. Rakstys, A. Abate, M. I. Dar, P. Gao, V. Jankauskas, G. Jacopin, E. Kamarauskas, S. Kazim, S. Ahmad, M. Grätzel, M. K. Nazeeruddin, *J. Am. Chem. Soc.* **2015**, *137*, 16172–16178.
- [16] M. Daskeviciene, S. Paek, Z. Wang, T. Malinauskas, G. Jokubauskaite, K. Rakstys, K. T. Cho, A. Magomedov, V. Jankauskas, S. Ahmad, H. J. Snaith, V. Getautis, M. K. Nazeeruddin, *Nano Energy* **2017**, *32*, 551–557.
- [17] I. Cho, N. J. Jeon, O. K. Kwon, D. W. Kim, E. H. Jung, J. H. Noh, J. Seo, S. I. Seok, S. Y. Park, *Chem. Sci.* **2017**, *8*, 734–741.
- [18] A. Krishna, D. Sabba, H. R. Li, J. Yin, P. P. Boix, C. Soci, S. G. Mhaisalkar, A. C. Grimsdale, *Chem. Sci.* **2014**, *5*, 2702–2709.
- [19] I. Zimmermann, J. Urieta-Mora, P. Gratia, J. Aragón, G. Grancini, A. Molina-Ontoria, E. Ortí, N. Martín, M. K. Nazeeruddin, *Adv. Energy Mater.* **2017**, *7*, 1601674.
- [20] F. Zhang, X. Zhao, C. Yi, D. Bi, X. Bi, P. Wei, X. Liu, S. Wang, X. Li, S. M. Zakeeruddin, M. Grätzel, *Dyes Pigm.* **2017**, *136*, 273–277.
- [21] S. Carli, J. P. Correa Baena, G. Marianetti, N. Marchetti, M. Lessi, A. Abate, S. Caramori, M. Grätzel, F. Bellina, C. A. Bignozzi, A. Hagfeldt, *ChemSusChem* **2016**, *9*, 657–661.
- [22] Y.-D. Lin, B.-Y. Ke, K.-M. Lee, S. H. Chang, K.-H. Wang, S. Huang, C.-G. Wu, P.-T. Chou, S. Jhulki, J. N. Moorthy, Y. J. Chang, K.-L. Liao, H.-C. Chung, C. Liu, S.-S. Sun, T. J. Chow, *ChemSusChem* **2016**, *9*, 274–279.
- [23] J. Burschka, A. Dualah, F. Kessler, E. Baranoff, N.-L. Cevy-Ha, C. Yi, M. K. Nazeeruddin, M. Grätzel, *J. Am. Chem. Soc.* **2011**, *133*, 18042–18045.
- [24] T. Leijtens, J. Lim, J. Teuscher, T. Park, H. J. Snaith, *Adv. Mater.* **2013**, *25*, 3227–3233.
- [25] T. Hasegawa, J. Takeya, *Sci. Technol. Adv. Mater.* **2009**, *10*, 024314.
- [26] S. Kazim, F. J. Ramos, P. Gao, M. K. Nazeeruddin, M. Grätzel, S. Ahmad, *Energy Environ. Sci.* **2015**, *8*, 1816–1823.
- [27] S. Cong, H. Yang, Y. Lou, L. Han, Q. Yi, H. Wang, Y. Sun, G. Zou, *ACS Appl. Mater. Interfaces* **2017**, *9*, 2295–2300.
- [28] J. Liu, Y. Wu, C. Qin, X. Yang, T. Yasuda, A. Islam, K. Zhang, W. Peng, W. Chen, L. Han, *Energy Environ. Sci.* **2014**, *7*, 2963–2967.
- [29] J.-S. Ni, H.-C. Hsieh, C.-A. Chen, Y.-S. Wen, W. T. Wu, Y.-C. Shih, K.-F. Lin, L. Wang, J. T. Lin, *ChemSusChem* **2016**, *9*, 3139–3144.
- [30] A. Abate, T. Leijtens, S. Pathak, J. Teuscher, R. Avolio, M. E. Errico, J. Kirkpatrick, J. M. Ball, P. Docampo, I. McPherson, H. J. Snaith, *Phys. Chem. Chem. Phys.* **2013**, *15*, 2572–2579.
- [31] J. H. Noh, N. J. Jeon, Y. C. Choi, M. K. Nazeeruddin, M. Grätzel, S. I. Seok, *J. Mater. Chem. A* **2013**, *1*, 11842–11847.
- [32] H. Zhang, Y. Shi, F. Yan, L. Wang, K. Wang, Y. Xing, Q. Dong, T. Ma, *Chem. Commun.* **2014**, *50*, 5020–5022.
- [33] J. Liu, S. Pathak, T. Stergiopoulos, T. Leijtens, K. Wojciechowski, S. Schumann, N. Kausch-Busies, H. J. Snaith, *J. Phys. Chem. Lett.* **2015**, *6*, 1666–1673.
- [34] C. Huang, W. Fu, C.-Z. Li, Z. Zhang, W. Qiu, M. Shi, P. Heremans, A. K.-Y. Jen, H. Chen, *J. Am. Chem. Soc.* **2016**, *138*, 2528–2531.
- [35] M. Franckevicius, A. Mishra, F. Kreuzer, J. Luo, S. M. Zakeeruddin, M. Grätzel, *Mater. Horiz.* **2015**, *2*, 613–618.
- [36] S. Ma, H. Zhang, N. Zhao, Y. Cheng, M. Wang, Y. Shen, G. Tu, *J. Mater. Chem. A* **2015**, *3*, 12139–12144.
- [37] C. Steck, M. Franckevicius, S. M. Zakeeruddin, A. Mishra, P. Bauerle, M. Grätzel, *J. Mater. Chem. A* **2015**, *3*, 17738–17746.
- [38] H.-C. Liao, T. L. D. Tam, P. Guo, Y. Wu, E. F. Manley, W. Huang, N. Zhou, C. M. M. Soe, B. Wang, M. R. Wasielewski, L. X. Chen, M. G. Kanatzidis, A. Fchetti, R. P. H. Chang, T. J. Marks, *Adv. Energy Mater.* **2016**, *6*, 1600502.
- [39] Y. Liu, Z. Hong, Q. Chen, H. Chen, W.-H. Chang, Y. Yang, T.-B. Song, Y. Yang, *Adv. Mater.* **2016**, *28*, 440–446.
- [40] F. Zhang, X. Liu, C. Yi, D. Bi, J. Luo, S. Wang, X. Li, Y. Xiao, S. M. Zakeeruddin, M. Grätzel, *ChemSusChem* **2016**, *9*, 2578–2585.
- [41] J. Alizon, J. Gallice, H. Robert, G. Delplanque, C. Weyl, C. Fabre, H. Strzelecka, *Mol. Cryst. Liq. Cryst. Mol. Cryst. Liq. Cryst.* **1976**, *33*, 91–100.
- [42] D. Chasseau, J. Gaultier, C. Hauw, R. Fugnitto, V. Gianis, H. Strzelecka, *Acta Crystallogr. B* **1982**, *38*, 1629–1631.
- [43] A. Bolag, M. Mamada, J.-I. Nishida, Y. Yamashita, *Chem. Mater.* **2009**, *21*, 4350–4352.
- [44] M. Courté, S. G. Surya, R. Thamankar, C. Shen, V. R. Rao, S. G. Mhaisalkar, D. Fichou, *RSC Adv.* **2017**, *7*, 3336–3342.
- [45] M. Courté, M. Alaeddine, V. Barth, L. Torteck, D. Fichou, *Dyes Pigm.* **2017**, *141*, 487–492.
- [46] S. Berny, L. Torteck, M. Véber, D. Fichou, *ACS Appl. Mater. Interfaces* **2010**, *2*, 3059–3068.
- [47] S. Berny, L. Torteck, D. Fichou, S. Matzen, J.-B. Moussy, *Appl. Phys. Lett.* **2010**, *97*, 253303.
- [48] B. Xu, E. Sheibani, P. Liu, J. Zhang, H. Tian, N. Vlachopoulos, G. Boschloo, L. Kloo, A. Hagfeldt, L. Sun, *Adv. Mater.* **2014**, *26*, 6629–6634.
- [49] D. A. da Silva Filho, V. Coropceanu, D. Fichou, N. E. Gruhn, T. G. Bill, J. Gierschner, J. Cornil, J.-L. Brédas, *Philos. Trans. R. Soc. London Ser. A* **2007**, *365*, 1435–1452.
- [50] T. Leijtens, I. K. Ding, T. Giovenzana, J. T. Bloking, M. D. McGehee, A. Sellinger, *ACS Nano* **2012**, *6*, 1455–1462.

Manuscript received: July 7, 2017

Revised manuscript received: July 10, 2017

Accepted manuscript online: July 10, 2017

Version of record online: August 10, 2017